ISSN: 0067-2904

Numerical Simulation of Double-Sided Lid-Driven Cavity Flow Using Moment-Based Boundary Conditions for The Lattice Boltzmann Method

Seemaa A. Mohammed
Department of mathematics, University of Baghdad, Baghdad, Iraq

Received: 25/3/2024 Accepted: 3/7/2024 Published: 30/6/2025

Abstract

The present study considers to confirming the applicability of flow with double-sided square lid driven cavity flow by using the lattice Boltzmann equation with moment-based boundary conditions for no slip boundaries. The boundary conditions are applied over the hydrodynamic moments of the lattice Boltzmann equations locally at each node. The investigation is carried out numerically for both single and multiple relaxation time models. To simulate two-sided lid driven-cavity flow, the top and bottom walls are moving with constant velocity while other walls are stationary. Various Reynolds numbers are used in a range of 100 and up to 5000. The present method shows the effect of the moving boundaries on the two symmetrical cavities that is separated by one center line. An expected behavior is achieved here. For validation, a comparison between our method and benchmark data is inserted. The comparison is found in a very good agreement with the literature.

Keywords: Lattice Boltzmann, moment-based boundary conditions, Two-sided cavity flow, MRT model

المحاكاة العددية لتدفق التجويف المتحرك بوجهين ويتم ذلك باستخدام شروط الزخم الحدودية لطريقة بولتزمان الشعرية

سيماء عبد الستار محمد

قسم الرياضيات ,كليه العلوم, جامعة بغداد, بغداد, العراق

الخلاصة

تهدف الدراسة الحالية إلى تأكيد قابلية تطبيق التدفق مع تدفق تجويفي مدفوع بغطاء مربع مزدوج الجوانب باستخدام معادلة بولتزمان الشبكية من خلال تطبيق شروط الحدود القائمة على السرعة الثابته. يتم إجراء هذا التأكيد باستخدام نموذجين من معادلة بولتزمان الشعرية. لمحاكاة تدفق التجويف المدفوع بالغطاء على الوجهين، تتحرك الجدران العلوية والسفلية بسرعة ثابتة بينما تكون الجدران الأخرى ثابتة. تم استخدام أرقام رينولدز المختلفة في نطاق من 100 وحتى 5000. الطريقة الحالية توضح تأثير الحدود المتحركة على التجويفين المتماثلين اللذين يفصل بينهما خط مركزي واحد. سلوك متوقع للمائع تم تحقيقه في هذا البحث. للتحقق من الحل، يتم إدراج مقارنة بين طريقتنا والبيانات الاخرى. لوحظ وجود توافق ممتاز مع البيانات المعيارية.

Email: Seemaa.a@sc.uobaghdad.edu.iq

1. Introduction

In recent years the lattice Boltzmann method (LBM) has proved to be a reliable method to simulate simple and complex flows [1-4]. This method has been developed to be an alternative to other conventional computational fluid dynamics (CFD), like in [5-7]. In the LBM the system develops by updating certain numbers of particle distribution functions at each site by streaming and collision steps. These functions propagate to the nearest nodes according to their lattice velocity then update their values at each time step in the local collision phase [8],[9]. By using the probability distribution functions, one can calculate easily the hydrodynamic moments and the pressure of the Navier-Stokes equations which is the main feature of the LBM. The first key to simulating any flow using the LBM is the numerical stability of the collision operator. Considerable and many collision models of the LBM are introduced during the development of this method. The simplest model is Bhatnagar-Gross-Krook (BGK) operator with one relaxation time [10-12]. The main generalization of the BGK model is obtained through d'Humiéres [13]. D'Humiéres introduced the multiple relaxation time (MRT) collision operator which provides higher numerical stability to the LBM especially when we simulate complex flows [14-16]. Together with the collision operator, the boundary conditions method is the main source of the stability of the LBM. The most commonly utilized is the bounce back method for no slip boundaries. In this method the distribution functions collide with the wall and reflect its direction to the fluid domain [17], [18]. A generalization has been carried out to the bounce-back method to overcome the lack of numerical stability also to apply it to slip regime, like in [19-22]. Similar to the work of Noble *et al.* [23], Bennett [24] extended this work from hexagonal model to a model of 9 lattice velocities. The method is called'' Moment based boundary conditions''. On the contrary to the bounce-back, the moment method is imposed directly on the lattice site. This method has proved its accuracy in the investigation of various flows for slip and no slip boundaries, like in [25-29].

Studies of one-sided lid-driven cavity flow were the subject of enormous methods to assess the efficiency of various numerical methods. Some of authors used the LBM to simulate this flow with accurate and successful simulations [27] [30-32]. Whereas other researchers employed the traditional (CFD), like in [33-35]. Recently, the two-sided lid-driven cavity flow has attracted some attention. An earlier experiment was done by Kuhlman *et al.* [36] to simulate double sided cavity flow with diverse aspect ratio which is considered as an extended to the one side of this flow. In the same matter of various aspect ratios, [37], [38] used the LBM to simulate this flow. In the meantime, Blohm and Kuhlmann [39] investigated experimentally this flow in a rectangular domain. Parallel and anti-parallel motion of the two-sided cavity flow were studied by Perumal and Dass in [40] and [41]. In this article an investigation of two-sided lid-driven cavity flow by using lattice Boltzmann method with moment method is achieved.

This article is organized as follows: In Section 2 we explain the methodology of finding the BGK-LBE. Section 3 gives the algorithm of the MRT model. In Section 4, the moment-based boundary conditions are presented whilst in Section 5 numerical simulations are given. Finally, a conclusion to this work is given in Section 6.

2. 2D incompressible BGK- lattice Boltzmann model

The D2Q9 discrete Boltzmann equation for the particle distribution functions $f_i, i = 0, \dots, 8$ is given by [8],

$$\frac{df_i}{dt} + \boldsymbol{\xi}_i . \nabla f_{\mathrm{i}} = -\frac{1}{\tau}\left(f_i - f_i^{(0)}\right). \quad (1)$$

As shown in Figure 1, D2Q9 model contains 9 particle velocities $\boldsymbol{\xi}_i$ where the distribution functions streaming according to the direction of the lattice velocity. This procedure is described in the left side of Equation (1). The right-hand side is the collision term where f_i moves towards their local equilibria $f_i^{(0)}$ over one relaxation time τ. The equilibrium function that truncated up to the second order of Mach number is given by, [42]

$$f_i^{(0)}(\mathbf{x}, \mathrm{t}) = \omega_i \, \rho\left(1 + \frac{\boldsymbol{\xi}_i.\boldsymbol{u}}{c_s^2} + \frac{(\boldsymbol{\xi}_i.\boldsymbol{u})^2}{2c_s^4} - \frac{\boldsymbol{u}^2}{2c_s^2}\right), \tag{2}$$

where the speed of sound $c_s^2 = 1/3$ and $\omega_0 = 0, \omega_{1,2,3,4} = 1/9$ and $\omega_{5,6,7,8} = \frac{1}{36}$ are the weights.

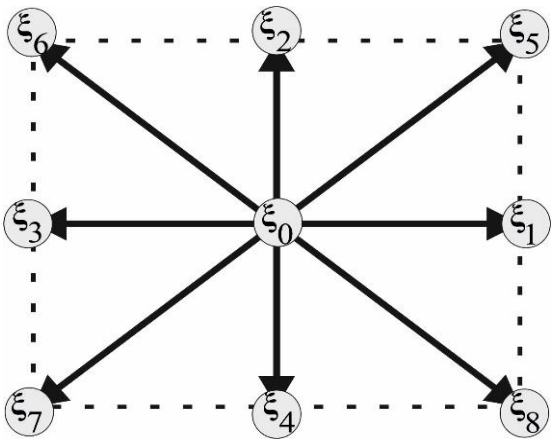

Figure 1: The D2Q9 lattice Boltzmann model.

At each lattice the three macroscopic moments, mass, momentum and momentum flux are defined as

$$\rho = \sum_{i=0}^{8} f_i \, ; \qquad \rho \boldsymbol{u} = \sum_{i=0}^{8} f_i \, \xi_{i\alpha} \quad ; \quad \Pi_{\alpha\beta} = \sum_{i=0}^{8} f_i \, \xi_{i\alpha} \xi_{i\beta,} \tag{3}$$

where the cartesian components α and β are used to define the velocity vector and the shear tensor in Equation (3).

The Navier-Stokes equations can be obtained easily by taking the first three moments of Equation (1) then applying the Chapman-Enskog expansion [43] and truncating the expansion up to leading order in relaxation rate to get

$$\partial_t \, \rho \, + \nabla . \rho \boldsymbol{u} = 0, \tag{4}$$

$$\partial_t \boldsymbol{\Pi} + \nabla . \left(\boldsymbol{\Pi}^{(0)} + \tau \boldsymbol{\Pi}^{(1)}\right) = \mathbf{0}. \tag{5}$$

Where $\boldsymbol{\Pi}^{(0)} = \sum_{i=0}^{8} f_i \, \boldsymbol{\xi}_i \boldsymbol{\xi}_i$ is the equilibrium momentum flux and $\boldsymbol{\Pi}^{(1)}$ is the first order correction of the momentum flux tensor

$$\boldsymbol{\Pi}^{(0)} = \frac{\rho}{3} \boldsymbol{I} + \rho \boldsymbol{u} \boldsymbol{u}. \tag{6}$$

$$\boldsymbol{\Pi}^{(1)} = -\frac{\rho}{3} (\nabla \mathbf{u} + (\nabla \mathbf{u})^{\mathbf{T}}) + \mathrm{O}(Ma^3). \tag{7}$$

The Mach number $Ma \ll 1$, $\boldsymbol{I}$ is the identity matrix and the kinematic viscosity in Equation (5) is $\nu = \tau/3$.

Now, to find the lattice Boltzmann equation, integrating Equation (1) over a characteristic for time gives

$$f_i(\boldsymbol{x} + \boldsymbol{\xi}_i \Delta t, t + \Delta t) - f_j(\boldsymbol{x}, t) = -\frac{\Delta t}{2\tau}\left(f_i(\boldsymbol{x} + \boldsymbol{\xi}_i \Delta t, t + \Delta t) - f_i^{(0)}(\boldsymbol{x}, t)\right) - \frac{\Delta t}{2\tau}\left(f_i(\boldsymbol{x}, t) - f_i^{(0)}(\boldsymbol{x}, t)\right) + \mathrm{O}(\Delta t^3). \tag{8}$$

The left-hand side of Equation (8) is obtained exactly while to find the integration for the right-hand side the Trapezoidal rule has been applied. Equation (8) is a second order implicit system of equations which is difficult to be approximate. Alternatively, an explicit algorithm was proposed by He et al. [44]

$$\overline{f}_i = f_i(\boldsymbol{x}, t) + \frac{\Delta t}{2\tau}\Big(f_i(\boldsymbol{x}, t) - f_i^{(0)}(\boldsymbol{x}, t)\Big). \tag{9}$$

Thus, the lattice Boltzmann equation in terms of $\overline{f}_i$ is obtained

$$\overline{f}_i(\boldsymbol{x} + \boldsymbol{\xi}_i\Delta t, t + \Delta t) - \overline{f}_i(\boldsymbol{x}, t) = -\frac{\Delta t}{\left(\tau + \frac{\Delta t}{2}\right)}\Big(\overline{f}_i(\boldsymbol{x}, t) - \bar{f}_i^{(0)}(\boldsymbol{x}, t)\Big) + O(\Delta t^3). \tag{10}$$

Equation (9) can be employed to compute the hydrodynamic quantities in terms of $\overline{f}_i$ as

$$\rho = \sum_{i=0}^{8} f_i = \sum_{0}^{8} \overline{f}_i \ ; \tag{11}$$

$$\rho\boldsymbol{u} = \sum_{i=0}^{8} f_i\,\boldsymbol{\xi}_i = \sum_{i=0}^{8} \overline{f}_i\,\boldsymbol{\xi}_i \ ; \tag{12}$$

$$\sum_{i=0}^{8} \overline{f}_i\,\boldsymbol{\xi}_i\boldsymbol{\xi}_i = \left(\frac{2\tau + \Delta t}{2\tau}\right)\boldsymbol{\Pi} - \frac{\Delta t}{2\tau}\boldsymbol{\Pi}^{(0)} \ . \tag{13}$$

Note that the ratio between grid spacing Δx to time step Δt is equal to $\frac{\Delta t}{\Delta x} = 0.1$.

3. **Multiple relaxation time model for LBM**

For higher Reynolds numbers, the BGK-LBM suffers from lack of numerical stability so (MRT) collision operator will be used instead [13], [14], [16], and [45]. In this work we will follow Dellar [16] by forming orthogonal basis Hermite polynomials. Since the D2Q9 model will be used, we need nine vectors. The first six lattice vectors are $\rho, \rho\,\boldsymbol{u}$ and the three vectors of the momentum flux $\boldsymbol{\Pi}$. The last three components are obtained from the orthogonal weighted lattice vectors, [16]

$$g_i = (1, -2, -2, -2, -2, 4, 4, 4, 4)^{\mathrm{T}}, \tag{14}$$

$$g_i\,\xi_{ix} = (0, -2, 0, 2, 0, 4, -4, -4, 4)^{\mathrm{T}}, \tag{15}$$

$$g_i\,\xi_{iy} = (0, 0, -2, 0, 2, 4, 4, -4, -4)^{\mathrm{T}}, \tag{16}$$

where T indicates transpose operator.

The corresponding "ghost moments" are introduced as

$$\mathcal{H} = \sum_{i=0}^{8} g_i f_i \ ; \qquad \boldsymbol{\mathcal{L}} = \sum_{i=0}^{8} g_i\boldsymbol{\xi}_i\, f_i \ . \tag{17}$$

The equilibrium of the "ghost moments" $\mathcal{H}^0 = \mathcal{L}_\alpha^0 = 0$. The ghost moments are linked to the third and fourth order non-hydrodynamic moments of D2Q9 model as

$$Q_{xxy} = \sum_{i=0}^{8} f_i\,\boldsymbol{\xi}_{ix}\,\boldsymbol{\xi}_{ix}\boldsymbol{\xi}_{iy} = \frac{1}{3}\rho u_y + \frac{1}{6}\,\mathcal{L}_y,$$

$$Q_{xyy} = \sum_{i=0}^{8} f_i\,\boldsymbol{\xi}_{ix}\,\boldsymbol{\xi}_{iy}\boldsymbol{\xi}_{iy} = \frac{1}{3}\rho u_x + \frac{1}{6}\,\mathcal{L}_x,$$

$$R_{xxyy} = \sum_{i=0}^{8} f_i\,\boldsymbol{\xi}_{ix}\,\boldsymbol{\xi}_{ix}\,\boldsymbol{\xi}_{iy}\boldsymbol{\xi}_{iy} = -\frac{1}{9}\rho + \frac{1}{3}\Pi_{xx} + \frac{1}{3}\Pi_{yy} + \frac{1}{9}\,\mathcal{H}. \tag{18}$$

Noting, one can obtain the zero and first order moments equations from the ghost variables. Different relaxation times will be chosen for the non-conserved moments that relax to their equilibria separately according to their own rates. By using Equation (10), one can compute the three post-collisional moments for MRT model in terms of $\overline{f}_i$ as

$$\bar{\boldsymbol{\Pi}}^{\sim} = \bar{\boldsymbol{\Pi}} - \frac{\Delta t}{\tau + \frac{\Delta t}{2}}\left(\bar{\boldsymbol{\Pi}} - \boldsymbol{\Pi}^{(0)}\right);$$
$$\bar{\mathcal{H}}^{\sim} = \bar{\mathcal{H}} - \frac{\Delta t}{\tau_r + \frac{\Delta t}{2}}\left(\bar{\mathcal{H}} - \mathcal{H}^{(0)}\right); \quad (19)$$

$$\bar{\boldsymbol{\mathcal{L}}}^{\sim} = \bar{\boldsymbol{\mathcal{L}}} - \frac{\Delta t}{\tau_s + \frac{\Delta t}{2}}\left(\bar{\boldsymbol{\mathcal{L}}} - \boldsymbol{\mathcal{L}}^{(0)}\right).$$

The post collision velocity distribution function $\bar{f}_i$ can be proposed according to Equation (19) as

$$\bar{f}_i = \omega_i(\rho + 3\rho\boldsymbol{u}\,.\boldsymbol{\xi}_i + \frac{9}{2}\left(\bar{\boldsymbol{\Pi}}^{\sim} - \frac{\rho}{3}\mathbf{I}\right) : (\boldsymbol{\xi}_i\boldsymbol{\xi}_i - \frac{1}{3}\mathbf{I})) + \omega_i g_i(\frac{1}{4}\bar{\mathcal{H}}^{\sim} + \frac{3}{8}\boldsymbol{\xi}_i\bar{\boldsymbol{\mathcal{L}}}^{\sim}). \quad (20)$$

Noting, if $\tau = \tau_r$=τ_s then the BGK-LBE will be recovered.

4. Moment-based boundary conditions

The general idea of this method is to impose conditions upon three of the lattice Boltzmann moments then express them into conditions on the unknown distribution functions $\bar{f}_i$ or f_i. At each boundary there are three unknown functions. From each row in Table- 1 we pick one moment, in particular the hydrodynamic moments, and then apply conditions on these moments. Finally, solves the three independent equations to find the unknown functions. For moving straight no slip boundaries, the southern wall will be chosen as an example to explain the moment method.

Table 1: Combination of unknown at the north boundary

Moments	Combination of unknown at the south wall
$\bar{\rho}, \rho\bar{u}_y, \bar{\Pi}_{yy}$	$\bar{f}_2 + \bar{f}_5 + \bar{f}_6$
$\rho\bar{u}_x, \bar{\Pi}_{xy}, \bar{Q}_{xyy}$	$\bar{f}_5 - \bar{f}_6$
$\bar{\Pi}_{xx}, \bar{Q}_{xxy}, \bar{S}_{xxyy}$	$\bar{f}_5 + \bar{f}_6$

At this wall $\bar{f}_2, \bar{f}_5$ and $\bar{f}_6$ are unknown and need to be found. Three conditions will impose on each moment from each row in Table 1 in terms on barred f. The constraints will be no slip and no flux boundary condition. From the first and second rows we have the horizontal and vertical velocities respectively $\overline{u_x} = U_l$ and $\overline{u_y} = 0$ where U_l is a constant velocity. The third condition is $\bar{\Pi}_{xx} = \Pi_{xx}^{(0)}$. The tangential stress condition is found by truncating the Chapman-Enskog expansion into $O(\tau)$ such that $\Pi_{xx} \cong \Pi_{xx}^{(0)} + \tau\Pi_{xx}^{(1)}$. Since $\partial_x u_x = 0$ then from Equation (7), $\Pi_{xx}^{(1)} = 0$. For no slip moving boundary, the three conditions are

$$\overline{\rho u_x} = U_l; \quad \overline{\rho u_y} = 0\,; \text{ and } \quad \bar{\Pi}_{xx} = \frac{\rho}{3} + \rho U_l^2. \quad (21)$$

Solving the three equations in (21) given the three unknown functions

$$\bar{f}_2 = \bar{f}_1 + \bar{f}_3 + \bar{f}_4 + 2\left(\bar{f}_7 + \bar{f}_8\right) - \frac{\rho}{3} - \rho U_l^2,$$
$$\bar{f}_5 = -\bar{f}_1 - \bar{f}_8 + \frac{\rho}{6} + \frac{1}{2}\rho U_l(U_l^2 + 1),$$
$$\bar{f}_6 = -\bar{f}_3 - \bar{f}_7 + \frac{\rho}{6} + \frac{1}{2}\rho U_l(U_l^2 - 1). \quad (22)$$

The density is calculated from Equations (22) and the vertical velocity ρu_y, which equal to zero at the south wall, such that

$$\rho = \bar{f}_0 + \bar{f}_1 + \bar{f}_3 + 2\left(\bar{f}_2 + \bar{f}_5 + \bar{f}_6\right) + \rho\bar{u}_y.$$

At the corners, five distribution functions are unknows and need five moments to be found.

The no slip conditions will be applied. These moments are $\overline{\Pi}_{xx}, \overline{\Pi}_{yy}, \overline{\rho u_x}, \overline{\rho u_y}$ and the fifth moment is the zero-shear stress $\overline{\Pi}_{xy}$. For more details, see [25].

5. Numerical results and discussion for double-sided lid-driven cavity flow using LBM

In this section, an incomparable sequare cavity flow with top and bottom moving walls is studied. The investigation is carried out by using the LBM with moment boundary conditions from Section 4, see Figure 2.

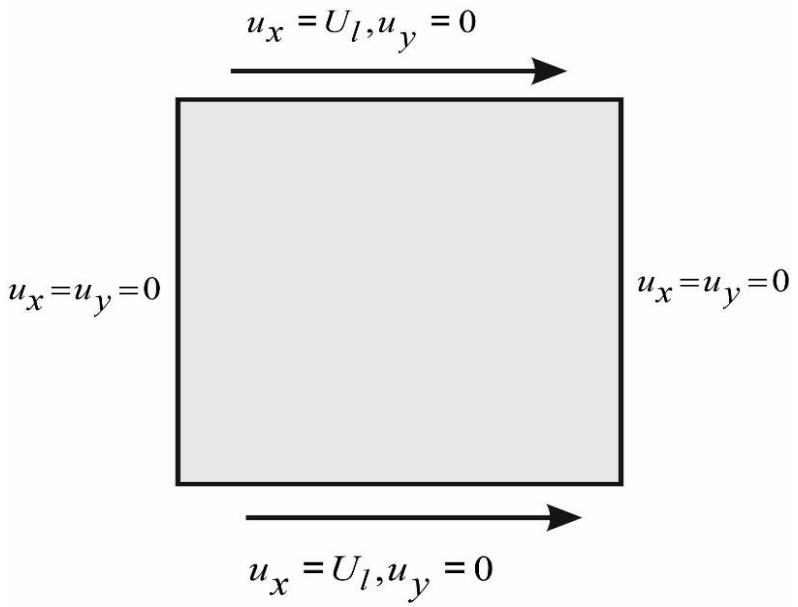

Figure 2: Geometry of double-sided parallel wall

In this work a Fortran 90 software is employed to simulate double-sided lid-driven cavity flow. Here, the dimensionless Reynolds number is defined as $\mathrm{Re} = U_l\, m/v$ where m is the number of grid points. The uniform velocity is chosen in lattice unit as $U_l = 0.1$. Various Reynolds numbers are studied in a range of $\mathrm{Re} = 100$ to $\mathrm{Re} = 5000$. Different lattice size is examined to test the accuracy of LBM. The simulations show that the convergence of the two-sided cavity flow is identical to the investigation of single lid cavity flow in [27]. The same challenge we faced which is the convergence of BGK-LBE with moment method for higher Reynolds numbers. For a sake of comparison, a grid resolution equal to $m \times m = 257 \times 257$ is used in this article for all Reynolds numbers. So, at Re= 100 and $Re = 400$ we apply the BGK-LBM while to achieve stability and more accuracy at $\mathrm{Re} = 1000, 1500, 2000$ and 5000, the MRT-LBM is applied. The two relaxation times of the ghost moments is chosen to be $\tau_r = \tau_s = \frac{\Delta t}{2}$ to ensure the distribution functions relax to their equilibrium separately and directly [16], [46]. The stream function φ is given to be

$$\varphi = \int -u_y dx + u_x dy.$$

Which satisfies the velocity components, [47]

$$u_x = \frac{\partial \varphi}{\partial_y},\ u_y = \frac{\partial \varphi}{\partial_x}.$$

A steady state is achieved if the following conditions is hold,

$$\max_{ij}\left|\varphi_{ij}^{(t+1)} - \varphi_{ij}^{(t)}\right| < 10^{-9}.$$

Figure 3 shows a stream line patterns for the top and bottom moving walls at different Reynolds numbers. The walls are moving with the same velocity. The two walls are moving from the left to the right. The two primary vortices cores are observed near the center of two halves of the lid driven cavity. These two counter-rotating stream functions are identical with a symmetry line separating between them horizontally in the middle of the domain at $x = 0.5$. For all Reynolds numbers the two cavities keep their symmetry in this flow. The two vortex cores of the primary vortices are slightly away from the middle of the cavities. However, by increasing the Reynolds number, the two cores are moving towards the center of the primary vortices. At $\mathrm{Re} > 100$ additional vortices formulate in the side of the two cavities. These counter-rotating secondary vortices are located at the right corner of each cavity. They placed exactly on the symmetry centre line. These symmetrical secondary vortices increase in size as Reynolds number increases. At $\mathrm{Re} = 5000$ the stream lines are combined again to create another secondary vortex at the top left of the upper cavity and at the lower left of the bottom one.

(a) Re=100 (b) Re=400

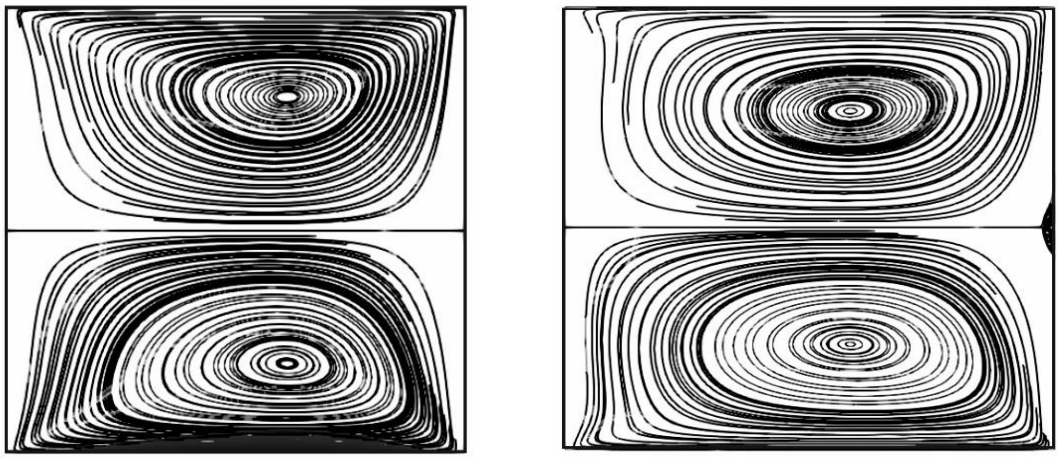

(c) Re=2000 (d) Re=5000

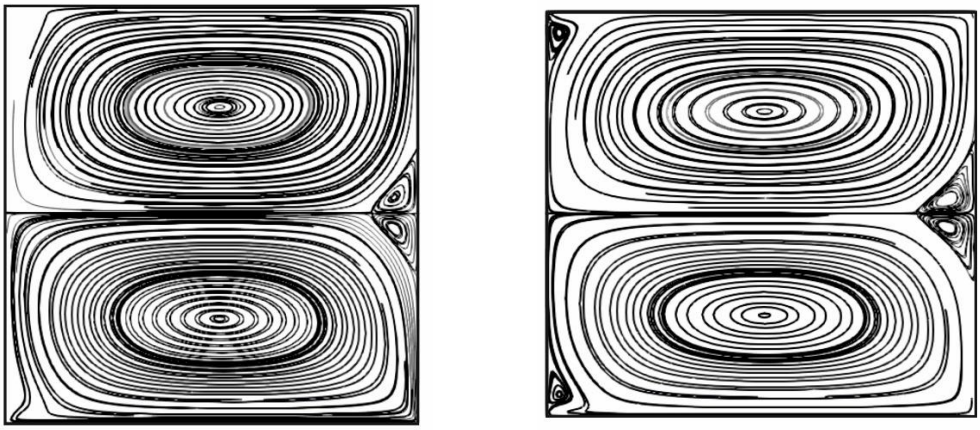

Figure 3: Streamlines pattern on 257x257 grid resolutions and various Reynolds numbers.

Figure 4 plots the vertical u_y and horizontal u_x velocity profiles, respectively. In these figures we consider various Reynolds numbers along the centrelines x and $y = 0.75$. This figure gives an expected behaviour. We notice that u_x, Figure 4 (a), take a parabolic shape symmetry about $y = 0.5$. This is due to location of the two cavities. The velocity u_x decreases until $y = 0.5$. Then it starts to increase again until reach to $u_x = 1$. On the other hand, the vertical velocity

u_y which is given in Figure 4 (b), increases slightly then decreases steadily down until passing the line $y = 0.8$ then it raises again. This behaviour is true for all Reynolds numbers. To show the whole picture of the velocity behaviour, in Figures 5 and 6 we plot the vertical and horizontal velocity profiles along various lines of x and y at $\mathrm{Re} = 400$ and 1000, respectively.

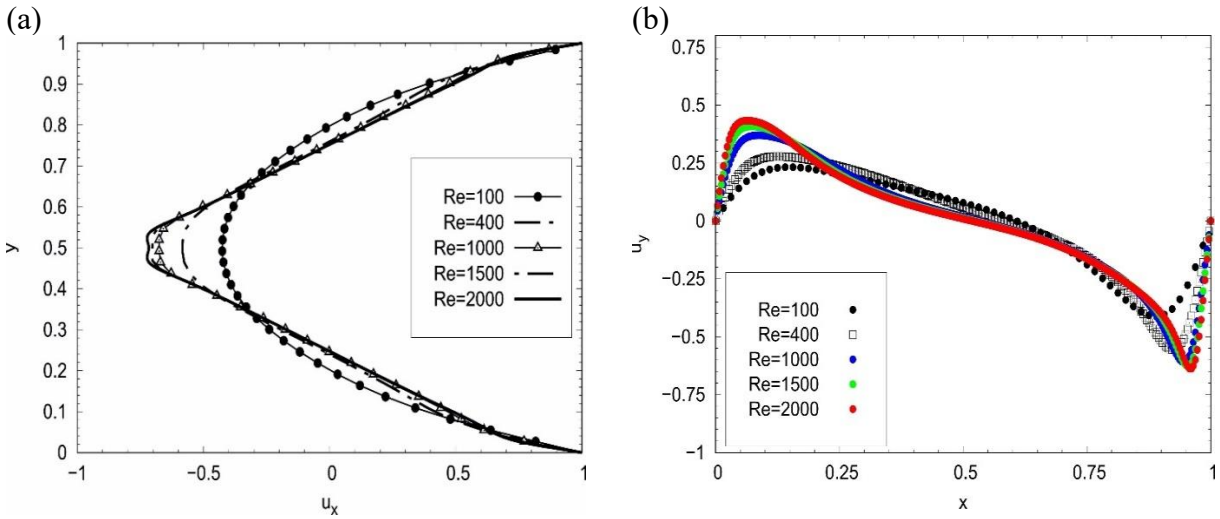

Figure 4: a A horizontal velocity $\boldsymbol{u_x}$ along $\boldsymbol{x = 0.5}$, and (b) A vertical velocity $\boldsymbol{u_y}$ through $\boldsymbol{y = 0.75}$ at different Reynolds numbers.

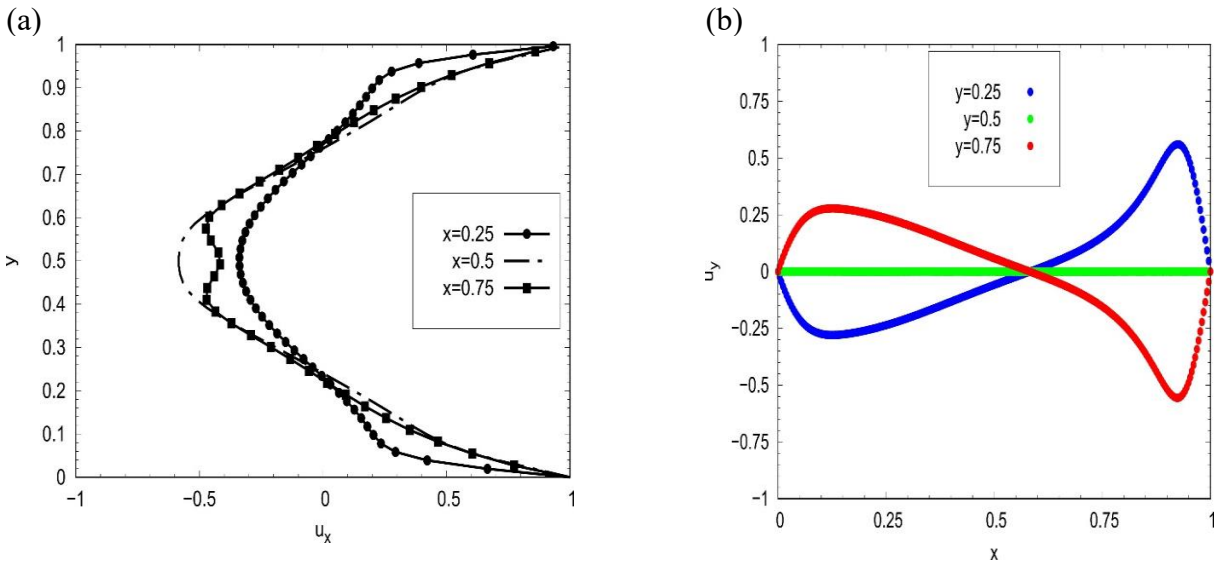

Figure 5: a A horizontal velocity $\boldsymbol{u_x}$ along $\boldsymbol{x = 0.25, 0.5}$ and 0.75, (b) A vertical velocity $\boldsymbol{u_y}$ through $\boldsymbol{y = 0.25, 0.5}$ and $\boldsymbol{0.75}$ at $\boldsymbol{\mathrm{Re} = 400}$.

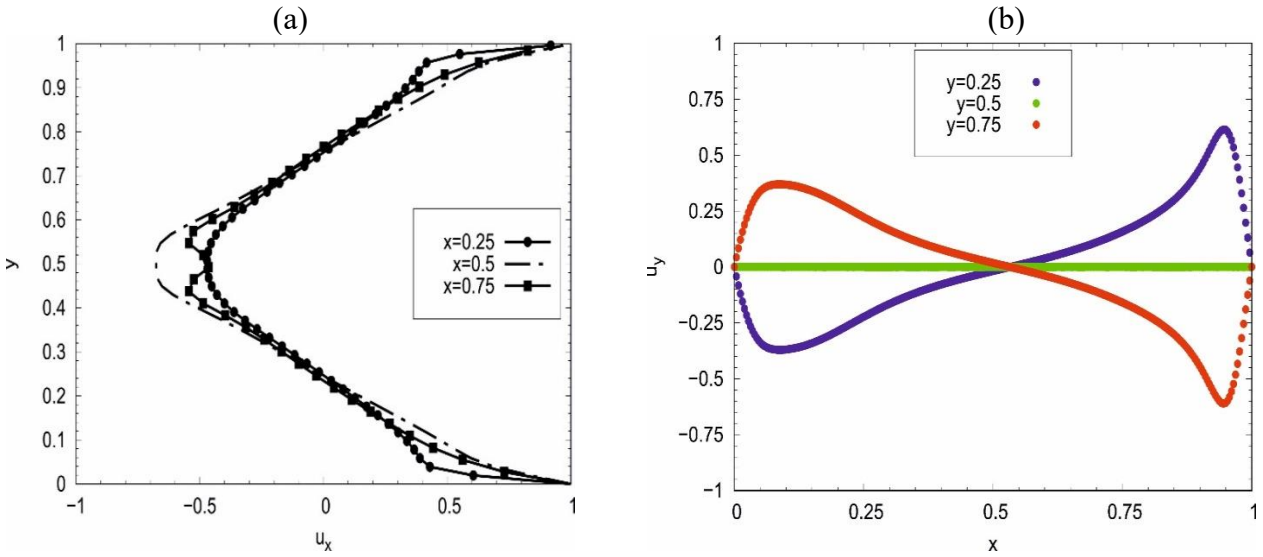

Figure 6: a A horizontal velocity $\boldsymbol{x = 0.25, 0.5}$ and 0.75, (b) A vertical velocity $\boldsymbol{u_y}$ through $\boldsymbol{y = 0.25, 0.5}$ and $\boldsymbol{0.75}$ at $\mathbf{Re = 1000}$.

The locations of the primary and secondary stream functions are listed in Table- 2. To validate our method, a comparison between our results with moment method and other methods in [40] is given. These methods are the LBM with bounce-back boundary conditions for stationary walls and equilibrium boundary for moving walls and the finite difference method (FDM). Table 2 shows a very good agreement between our results and those in [40]. Noting, since at $\mathrm{Re} = 100$ there is no secondary vortex so only the locations of the primary vortex are inserted.

Table 2: Comparisons of the locations of the primary and secondary vortices at different Reynolds numbers.

Re	The comparison	Primary vortex centre				Secondary vortex centre			
		Bottom		Top		Bottom		Top	
		x	y	x	y	x	y	x	Y
100	Present(LBM)	0.6171	0.2187	0.6170	0.7968	-	-	-	-
	LBM [40]	0.6145	0.2024	0.6145	0.7949	-	-	-	-
	FDM [40]	0.6146	0.2025	0.6145	0.7949	-	-	-	-
400	Present(LBM)	0.5859	0.2421	0.5859	0.7656	0.9921	0.4804	0.9921	0.5234
	LBM [40]	0.5845	0.2388	0.5845	0.7549	0.9875	0.4713	0.9874	0.5283
	FDM [43]	0.5844	0.2387	0.5844	0.7552	0.9872	0.4636	0.9872	0.5262
1000	Present(LBM)	0.5312	0.2500	0.5312	0.7578	0.9609	0.500	0.9609	0.4609
	LBM [40]	0.5314	0.2431	0.5314	0.7556	0.9528	0.4619	0.9528	0.5365
	FDM [40]	0.5352	0.2453	0.5352	0.755	0.9550	0.4572	0.9550	0.5408
1500	Present(LBM)	0.5234	0.2500	0.5234	0.7578	0.9492	0.4609	0.9492	0.5390
	LBM [40]	0.5234	0.2434	0.5234	0.7518	0.9434	0.4569	0.9433	0.5385
	FDM [40]	0.5245	0.2453	0.5267	0.7528	0.9444	0.4572	0.9443	0.5429
2000	Present(LBM)	0.5234	0.2500	0.5234	0.7578	0.9453	0.4609	0.9453	0.5390
	LBM [40]	0.5108	0.2489	0.5108	0.7497	0.9378	0.4598	0.9377	0.5389
	FDM [40]	0.5132	0.2474	0.5132	0.7528	0.9400	0.4573	0.9400	0.5478
5000	Present(LBM)	0.5078	0.2500	0.5078	0.7500	0.9375	0.4687	0.9375	0.5390
	LBM [40]	-	-	-	-	-	-	-	-
	FDM [40]	-	-	-	-	-	-	-	-

6. Conclusions

In this work double-sided lid driven cavity flow is computed. Simultaneously the lattice Boltzmann method with moment-based boundary condition is employed to simulate this flow. Both the BGK and a particular implementation of the MRT collision operator were applied with the moment method. The MRT schemer was used for higher Reynolds numbers to reach a numerical stability. Here, we studied the physics of the cavity flow when the north and the south walls are moving. Two cavities were appeared and for both of the them core the primary vortices moved to the centre with higher Reynolds numbers. Secondary vortices are visualized in the side of the two cavities for $\mathrm{Re} > 100$. An additional two counter-rotating stream functions were formed in the left side of the primary vortices. Horizontal and vertical velocity profiles are explained in graphs in details for different Reynolds numbers and locations. Meanwhile, the locations of the primary and secondary vortices centres are listed for various Re and compared with other works. A very good agreement was obtained.

References

[1] G. R. McNamara and G. Zanetti, "Use of the Boltzmann equation to simulate lattice-gas automata." *Physical Review Letters*, vol. 61, pp. 2332, 1988.

[2] S. Chen and G.D. Doolen, "Lattice Boltzmann method for fluid flows." *Annual review of fluid mechanics*, vol. 30, no. 1, pp. 329-364, 1998.

[3] X. Shan and H. Chen ,"Simulation of nonideal gases and liquid-gas phase transitions by the lattice Boltzmann equation," *Physical Review E*, vol. *49*, no. 4, p.2941, 1994.

[4] A.K . Gunstensen, D.H. Rothman, S. Zaleski and G. Zanetti," Lattice Boltzmann model of immiscible fluids," *Physical review A*, vol. 43, no. 8, p.4320, 1991.

[5] M.A. Murad and A.M. Abdulhadi, "Peristaltic transport of power-law fluid in an elastic tapered tube with variable cross-section induced by dilating peristaltic wave," *Iraqi Journal of Science*, vol. 62, no. 4, pp.1293-1306, 2021.

[6] M.S. Hussein," unsteady non-Newtonian fluid flow problem in plane solving by Mac method ", *Iraqi Journal of Science*, vol.53*,* no.3, 2012.

[7] J.A.A. Al-Hawasy and N.F. Mansour," The Galerkin-Implicit Method for Solving Nonlinear Variable Coefficients Hyperbolic Boundary Value Problem", *Iraqi Journal of Science*, pp.3997-4005, 2021.

[8] Z. Guo and C. Shu, *Lattice Boltzmann method and its applications in engineering*. World Scienti_c, *Company Incorporated*, 2013.

[9] S. Succi. *The lattice Boltzmann equation for fluid dynamics and beyond*. *Oxford University Press, UK*, 2001.

[10] P. L. Bhatnagar, E. P. Gross, and M. Krook," A model for collision processes in gases. I. Small amplitude processes in charged and neutral one-component system," *Physical review*, vol 94, no. 3, p 511, 1954.

[11] X. Shan, X.F. Yuan, and H. Chen, "Kinetic theory representation of hydrodynamics: a way beyond the Navier–Stokes equation," *Journal of Fluid Mechanics*, vol. 550, pp. 413–441, 2006.

[12] X. He and L. Luo," A priori derivation of the lattice Boltzmann equation," *Physical review* E, vol. **55**, no. 6, p. R6333 ,1997.

[13] D. d'Humiéres," Generalized lattice-Boltzmann equations," *Prog. Astronaut. Aeronaut.*, pp. 450–458, 1992.

[14] P. Lallemand and L.S. Luo," Theory of the lattice Boltzmann method: Dispersion, dissipation, isotropy, Galilean invariance, and stability," *Physical review E*, vol. 61, no. 6, p. 6546, 2000.

[15] P.J. Dellar," Incompressible limits of lattice Boltzmann equations using multiple relaxation times," *Journal of Computational Physics*, vol. 190, no. 2 , pp. 351–370, 2003.

[16] A. JC. Ladd,"Numerical simulations of particulate suspensions via a discretized Boltzmann equation. part 1. theoretical foundation", *Journal of Fluid Mechanics*, vol. 271, pp. 285–309, 1994.

[17] X. Y. He, Q. S. Zou, L. S. Luo, and M. Dembo," Analytic solutions of simple flows and analysis of nonslip boundary conditions for the lattice Boltzmann BGK model", *Journal of Statistical Physics*, vol. 87, pp. 115-136, 1997.

[18] YH. Qian, D. d'Humières, and P. Lallemand," Lattice BGK models for Navier-Stokes equation," *Europhysics letters*, vol. 17, no. 6, p.479, 1992.

[19] J.E. Broadwell," Study of rarefied shear flow by the discrete velocity method," *Journal of Fluid Mechanics*, vol. 19, pp.401–414, 1964.

[20] R. Gatignol," Kinetic theory boundary conditions for discrete velocity gases," *The Physics of Fluids,* vol. 20, no. 12, pp. 2022–2030, 1977.

[21] Q. Zou and X. He," On pressure and velocity boundary conditions for the lattice Boltzmann BGK model," *Phys. Fluids.*, 9:1591–1598, 1997.

[22] M. Bouzidi , M. Firdaouss and P. Lallemand ,"Momentum transfer of a Boltzmann-lattice fluid with boundaries," *Physics of Fluids,* vol. 13, no. 11, pp.3452–3459, 2001 .

[23] D.R. Noble, S. Chen, . G. Georgiadis, and R. O. Buckius," A consistent hydrodynamic boundary condition for the lattice Boltzmann method," *Physics of Fluids*, vol. 7, no.1, pp. 203–209, 1995.

[24] S. Bennett, *A lattice Boltzmann model for diffusion of binary gas mixtures*, PhD thesis, University of Cambridge, 2010.

[25] R. Allen and T. Reis,"Moment-based boundary conditions for lattice Boltzmann simulations of natural convection in cavities Progress in Computational Fluid Dynamics, an International Journal, vol. 16, no. 4, pp. 216–231, 2016.

[26] A. Hantsch, T. Reis and U. Gross," Moment method boundary conditions for multiphase lattice Boltzmann simulations with partially-wetted walls*," The Journal of Computational Multiphase Flows*, vol. 7, no. 1, pp. 1–14 ,2015.

[27] S. Mohammed and T. Reis, "Using the lid-driven cavity flow to validate moment-based boundary conditions for the lattice Boltzmann equation," *Archive of Mechanical Engineering*, vol. 64, no. 1, pp. 57–74 ,2017.

[28] T. Reis, " Burnett order stress and spatially-dependent boundary conditions for the lattice Boltzmann method," *Progress in Computational Fluid Dynamics, an International Journal Commun. Computational Physics,* vol. 27, pp. 167–197 ,2020.

[29] S. Mohammed and T. Reis," A Lattice Boltzmann method with moment-based boundary conditions for rarefied flow in the slip regime", *Physical review E*., vol. 104, no. 4, p. 045309, 2021.

[30] S. Hou, Q. Zou, S. Chen, G. D. Doolen, and A. C. Cogley,"Simulation of cavity flow by the lattice Boltzmann method" *Journal of computational physics*, vol. 118, no.2, pp.329 –347, 1995.

[31] Lai, G. Lin, L. & Huang, J., Accuracy and Efficiency study of a LBM for steady-state flow simulation. Num. Heat Transfer-B, 39, pp. 21–43, 2001.

[32] L.S. Luo,W. Liao, X. Chen,Y. Peng,W. Zhang ," Numerics of the lattice Boltzmann method: Effects of collision models on the lattice Boltzmann simulations," *Physical review E*, vol. 83, no. 5, p. 056710, 2011.

[33] U. Ghia, K.N. Ghia and C.T. Shin," High-resolutions for incompressible flow using the Navier-Stokes equations and a multigrid method," *Journal of computational physics*, vol. 48, no. 3, pp.387–411, 1982.

[34] M. Sahin and R.G. Owens," A novel fully implicit finite volume method applied to the lid-driven cavity problem—part i: High Reynolds number flow calculations," *International journal for numerical methods in fluids*, vol. 42, no. 1, pp.:57–77, 2003.

[35] O. Botella and R. Peyret," Benchmark spectral results on the lid-driven cavity flow," *Computers & Fluids*, vol. 27, no. 4, pp: 421–433, 1998.

[36] W. Kuhlmann and J. Rath ", Flow in 2-sided lid-driven cavities: nonuniqueness, instability, cellular structures," *Journal of Fluid Mechanics*, vol. 336, pp:267–299, 2001.

[37] N.C. Sidik and S.A. Razali," Various speed ratios of two-sided lid-driven cavity flow using lattice Boltzmann method," *Journal of Advanced Research in Fluid Mechanics and Thermal Sciences*, vol. 1, no. 1, pp:11-18, 2014.

[38] A. Kumar and S. P. Agrawal," Mathematical and simulation of lid driven cavity flow at different aspect ratios using single relaxation time lattice Boltzmann technique," *American Journal of Theoretical and Applied Statistics*, vol. 2*,* no. 3, pp:87-93, 2013.

[39] H. Blohm and C. Kuhlmann, "The two-sided lid-driven cavity: experiment on stationary and time-dependent flows," *Journal of Fluid Mechanics*, vol. 450, pp: 67–95, 2002.
[40] D.A. Perumal and A.K. Dass," *Simulation of flow in two-sided lid-driven square cavities by the lattice Boltzmann method,"* vol. 59, p. 45, WIT Press, , 2008.
[41] D.A. Perumal and A.K. Dass," Simulation of Incompressible Flows in Two-Sided Lid-Driven Square Cavities: Part I-FDM", *CFD Letters*, vol. *2,* no. 1, pp.13-24, 2010.
[42] X. He and L-S Luo, "Theory of the lattice Boltzmann method: from the Boltzmann equation to the lattice Boltzmann equation," *Physical Review E,* vol. 56, no. 6, p. 6811, 1997.
[43] S. Chapman and Th. G. Cowling, *The mathematical theory of non-uniform gases: an account of the kinetic theory of viscosity, thermal conduction and diffusion in gases*, (Cambridge University Press, Cambridge, England, 1970.
[44] X. He, X. Shan and G.D. Doolen," Discrete Boltzmann equation model for nonideal gases," *Physical Review E*, vol. 57:R13, no. 1, 1998.
[45] D. D'Humieres and I. Ginzburg,"Viscosity independent numerical errors for lattice Boltzmann models: from recurrence equations to magic collision numbers," *Computers & Mathematics with Applications*, vol. 58, no. 5, pp. 823-840, 2009.
[46] P. J Dellar," Nonhydrodynamic modes and a priori construction of shallow water lattice Boltzmann equations," *Physical Review E*, vol. 65, pp. 036309, 2002.
[47] J. R. Toro and S. Pedraza,"*Flow evolution mechanisms of lid-driven cavities*," In *Hydrodynamics-Advanced Topics*. Intech Open, 2011.